High performance thin-film optical filters with stress compensation

Thomas Begou, Fabien Lemarchand, Frédéric Lemarquis, Antonin Moreau, Julien Lumeau

High performance thin-film optical filters with stress compensation

THOMAS BEGOU[1], FABIEN LEMARCHAND[1], FREDERIC LEMARQUIS[1], ANTONIN MOREAU[1] AND JULIEN LUMEAU[1*]

[1] *Aix Marseille Université, CNRS, Centrale Marseille, Institut Fresnel, Marseille, France*
**julien.lumeau@fresnel.fr*

Abstract: We present a thorough description of high performance thin-film optical filters with high flatness. These components can combine several tens or hundreds of layers and are manufactured using plasma-assisted reactive magnetron sputtering. Stress compensation is achieved using dual side coatings with appropriate spectral function. Examples of highly reflecting mirrors at 515 nm with 15 nm flatness peak-to-valley over up to 75 mm diameter aperture, narrow bandpass filters and filters with broadband controlled transmission are described.

1. Introduction

With the recent advances of the physical vapor deposition technologies, especially magnetron sputtering technique, it is now more and more common to fabricate very thick coatings with total thickness of several micrometers or tens of micrometers. With these energetic technologies, very dense layers are produced. As a consequence, the produced coatings are more and more resistant in harsh conditions but high residual stress is then generally observed in the layers [1]. In most of the coatings produced with oxide materials, this high residual stress is generally not a problem from an adhesion point of view (delamination can generally be avoided by combining the proper materials), but it can induce large substrate deformation that scale with the substrate diameter and the square of the thickness of the substrate [2,3]. While such deformation is not a major problem for transmitting elements, this becomes a major issue when working with reflected wavefront or with complex optical systems. In order to overcome these limitations, it is either possible to work on the mitigation of individual layer stress level [4,5], the mitigation of stress-induced deformation [6,7] or to perform stress compensation using dual side coatings with different optical functions [8-10]. Using the last approach, these coatings may even be designed to be athermal, i.e. to work over a broad temperature range [11]. Moreover, in the literature, there is little or no clear description of the actual performances that can be achieved with such an approach. In this paper, we thus provide a complete description of the fabrication of various kinds of optical elements with stress compensation. These results rely on the repeatable and accurately determined stress coefficients of Nb_2O_5, HfO_2 and SiO_2 [12] as obtained with plasma assisted reactive magnetron sputtering. Highly reflecting mirrors at 515 nm with 15 nm flatness peak-to-valley over up to 75 mm diameter aperture that were fabricated for integration on the laser beam circulator of the ELI-NP (Extreme Light Infrastructure – Nuclear Physics) are first presented. We then show how this approach can then be extended to more complex filters: bandpass filters (narrow or broadband) or filters with custom shapes such as intensity equalizing filters.

2. Methodology

In this work, we studied different types of components including highly reflecting mirrors, bandpass filters and filters with broadband controlled transmission. Depending on their complexity, the filters were designed either analytically using classical quarter wave formulae (mirrors or narrow bandpass filters) or numerically using needle optimization technique

through Optilayer software [13-15] (visible bandpass filters and filters with custom shapes). In this study, all the components were fabricated on fused silica substrates. High index materials were either Nb_2O_5 or HfO_2 and low index material was SiO_2.

For each of the studied filters, we calculated the deformation associated with the multilayer stack. For this calculation, we implemented Stoney equation [2]:

$$\boldsymbol{\sigma = \frac{E_S {d_S}^2}{6 t_f (1 - \upsilon_S)} \left(\frac{1}{R_{S+f}} - \frac{1}{R_S} \right)} \tag{1}$$

where E and ν_s stand respectively for the Young modulus and the Poisson coefficient of the substrate. In our case, for fused silica we used E_s = 73 GPa and ν_s = 0.16. R_S and R_{S+f} are the radius of curvature respectively before and after deposition of the multilayer stack and d_S is the substrate thickness.

This equation can be re-written to account for different materials and multilayer structures:

$$R_{S+f} = \frac{{d_S}^2 K_S R_S}{{d_S}^2 K_S + R_S \left(\sum_{i=1}^{N_H} \sigma_H(d_{Hi}) d_{Hi} + \sum_{j=1}^{N_L} \sigma_L(d_{Lj}) d_{Lj} \right)} \tag{2}$$

where $\sigma_X(d_{Xi})$ is the stress coefficient of the layer #i, N_X, the total number of layers and d_{Xi}, the thickness the layer #i. Finally, X stands for the high (H) and low (L) refractive index materials, and:

$$K_S = \frac{E_S}{6(1 - \upsilon_S)} \tag{3}$$

K_S is a constant term that depends on the mechanical properties of the substrate. Stress compensation was achieved using dual side coating with similar approach as for the one presented in [9]. For this, we designed structures that allow securing the same stress-induced deformation on each face, i.e.:

$$\left(\sum_{i=1}^{N_H} \sigma_H(d_{Hi}) d_{Hi} + \sum_{j=1}^{N_L} \sigma_L(d_{Lj}) d_{Lj} \right)_{Face\ A} = \left(\sum_{i=1}^{N_H} \sigma_H(d_{Hi}) d_{Hi} + \sum_{j=1}^{N_L} \sigma_L(d_{Lj}) d_{Lj} \right)_{Face\ B} \tag{4}$$

In other words, when designing the structures that will be coated on each face of the substrates, we did not only consider spectral performances of the components but also stress-induced deformation. The stress coefficient values that were determined previously [12] were directly implemented for this work. These stress coefficients are equal to:

- $-76.4 \times d_{HfO2} + 0.0178$ MPa for HfO_2
- $-61 \times d_{Nb2O5} - 0.0003$ MPa for Nb_2O_5
- $-371.2 \times d_{SiO2} - 0.0360$ MPa for SiO_2

and were determined with a precision within ± 5 MPa (d_{HfO2}, d_{Nb2O5} and d_{SiO2} stands respectively for the thickness of HfO_2, Nb_2O_5 and SiO_2 layers and are given in nanometers).

As the designed filters were quite complex, the precise control of the thickness of each layer had to be carried out using optical monitoring. Prior to deposition, optical monitoring strategy was determined using in-house software [16]. The implemented approach consisted in minimizing the number of monitoring glasses in order to benefit for possible errors compensation and change test glasses when thickness errors start diverging. All strategies were then tested using virtual deposition process and fabrication was carried out only after such theoretical analysis.
All the studied components were then fabricated using a Bühler HELIOS machine where low and high refractive index materials were both deposited through Plasma Assisted Reactive Magnetron Sputtering (PARMS). The main chamber is subdivided into different treatment zones, two dedicated for dielectric materials (MF magnetron sputtering), and one for oxygen plasma assistance (PBS). The substrates are set on a 12-position rotating sample holder (rotation at 240 rpm). According to the deposited material, either low or high index, the corresponding MF magnetron sputtering cathode is switched on. The oxygen plasma assistance is used for densification of the coating and also to produce stoichiometric layers. Typical deposition rates of low and high index materials are respectively around 0.40-0.45 $nm.s^{-1}$ and 0.50-0.60 $nm.s^{-1}$. The control of the thickness of each of the layers was carried out using an OMS 5100 optical monitoring system.

After fabrication, different types of measurements were performed:

- Transmittance and reflectance were measured using a Perkin Elmer Lambda 1050. Measured spectral range was adapted based on the spectral specifications of the filters.
- Flatness of the components was measured using a Zygo NewView 7300 optical profilometer. This system based on low coherence interferometry allows separating the contribution of each face and therefore accurately and independently mapping the flatness of each of the components. By implementing a calibration of the measurement before measuring the fabricated samples, an accuracy of ± 5 nm could be achieved for samples up to 75 mm diameter.
- Finally, when required, uniformity of the components was measured using a custom measurement system [17].

3. Experimental Results

2.1 Highly reflecting mirrors

ELI-NP is a European-funded infrastructure build in Romania aiming at providing scientists with a very high power laser chain for nuclear physics experiments [18]. Within this facility, a laser beam circulator had to be installed for the generation of a high brilliance gamma beam [19]. This circulator, originally developed by CNRS-LAL and ALSYOM, includes a large number of mirrors for the circulator itself (64) but also in the beam delivery arm [20]. These mirrors are highly reflecting mirrors for 515 nm, working at oblique incidence (between 15° and 45°, depending on the mirrors), with diameter between 30 and 75 mm, and with a required flatness better than λ/30 peak-to-valley at 515 nm over 85% aperture. Table 1 provides a list of the mirrors that were fabricated within this project.

Table 1. Specifications of the ELI-NP laser beam circulator mirrors.

Wavelength, nm	AOI, °	Reflection	Thickness, nm	Aperture, mm	Flatness PTV
515	22.5	> 99.95%	10	30	λ/20 (λ/30 over 80% aperture)
515	45	> 99.95%	13	50.8	λ/20 (λ/30 over 75% aperture)

515	15	> 99.95%	19	76.2	λ/20 (λ/30 over 60% aperture)
515	45	> 99.95%	19	76.2	λ/20 (λ/30 over 60% aperture)

The first flatness in Table 1 is the one required over a 90+% aperture and the one into bracket over a reduced aperture. The structures that match these specifications were designed and the number of layers and the total stack thickness are summarized in Table 2. High refractive index material is HfO_2 and low index material is SiO_2. Mirrors at 15° and 22.5° are quarterwave mirrors at 530 nm to account for the spectral shift with incidence and the mirrors at 45° are periodic quarterwave mirrors with matched layers for 45°.

Table 2. Typical parameters of the designed mirrors.

Function	AOI, deg	Number of layers	Total thickness, nm
Mirror	15	33	2556.85
Mirror	22.5	33	2556.85
Mirror	45	37	3068.78
Antireflection coating	15	3	427.8
Antireflection coating	45	9	584.3

Efficient optical monitoring based on a single monitoring wavelength corresponding to one of the edges of the main reflection lobe was implemented for the control of the optical thickness of each layer of the stack. Figure 1 shows the spectral dependence of the reflection coefficient measured, on a mirror that was designed for 22.5° angle of incidence. One can see that close to theoretical performances were achieved using this optical monitoring strategy. However, using this instrument, we could not precisely characterize the maximum reflectivity due to a limited measurement precision. Therefore, we used a NovaWave LossPro measurement system based on Cavity Ring-Down Laser technique to precisely characterize the reflection coefficients for both polarizations [21].

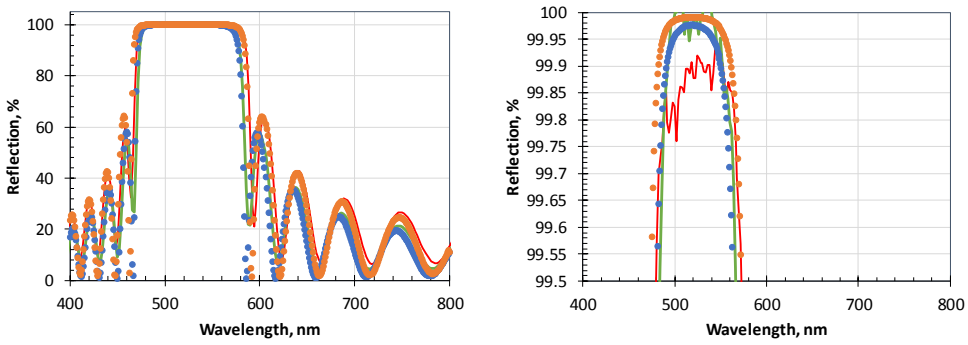

Figure 1. Spectral dependence of reflection at 22° angle of incidence for s polarization (theory in orange and experimental in red) and p polarization (theory in blue and experimental in green) in case of single side coated mirrors.

The configuration of this system is fixed and cannot perform measurement at each of the necessary angles of incidence. 15° and 22° mirrors were measured at 30° angle of incidence and mirrors for 45° were measured at the requested angle of incidence. In addition, we could not measure the mirrors at 515 nm but at 532 nm as the laser used in this system is a frequency doubled Nd:YAG laser. Table 3 provides a theoretical comparison of the reflection coefficient at 30° for both polarizations in case of 15° and 22.5° as well as the expected reflection coefficient for the mirrors at 45°.

Table 3. Theoretical reflection coefficients of the different mirrors for different incidence wavelengths and incidence angles.

Mirrors at 15°				
	s		**p**	
	30°	**15°**	**30°**	**15°**
515 nm	99.998	99.996	99.987	99.993
532 nm	99.996	99.996	99.97	99.994
Mirrors at 22.5°				
	s		**p**	
	22.5	**30**	**22.5**	**30**
515 nm	99.998	99.997	99.992	99.987
532 nm	99.998	99.996	99.99	99.969
Mirrors at 45°				
	s		**p**	
	45°		45°	
515 nm	99.99		99.98	
532 nm	99.99		99.965	

One can see that for each of the measurement configurations, the reflection coefficient is mildly changed and stays above 99.95%. In addition, due to the very good agreement between theoretical and experimental reflection curves, one can expect that by a simple comparison between these reflection coefficients at 532 nm and 30° angle of incidence, it is possible to simply recalculate the performances of the mirrors at 515 nm and 15° or 22.5° angle of incidence. The performances of the mirrors at 45° of incidence were measured at the same incidence but at 532 nm and the reflection at 515 nm was recalculated. Each of the fabricated mirrors was characterized and we summarized in Table 4, the average performances of the fabricated mirrors.

Table 4. Estimated performances at 515 nm deduced from measurements à 532 nm.

Number of fabricated mirrors		**Rs**	**Rp**
AOI = 15°			
11	Mean	99.963	99.951
	STDV	0.003	0.002
AOI = 22.5°			
80	Mean	99.967	99.962
	STDV	0.005	0.007
AOI = 45°			
31	Mean	99.976	99.952
	STDV	0.003	0.004

Measured reflection coefficients are very similar for all the 80 mirrors designed for 22.5 and less than 10 were out of the specifications with a value of R_P not lower than 99.93%. It is worth noting that the measured reflection coefficients are lower than the theoretically predicted values. It can be shown that this difference is mostly due to the residual surface scattering of the substrate and additional tests with samples with lower roughness allowed demonstrating that reflection can further be increased by 0.02% or more.

The second challenge when fabricating these mirrors consisted of fabricating mirrors with very high flatness. For part of the samples, stress compensation was achieved by depositing

an identical mirror on the substrate rear face. 60 mirrors for 22.5° angle of incidence and with a diameter of 30 mm were fabricated using exactly the same design. Figure 2 shows an example of flatness measurement performed on a mirror.

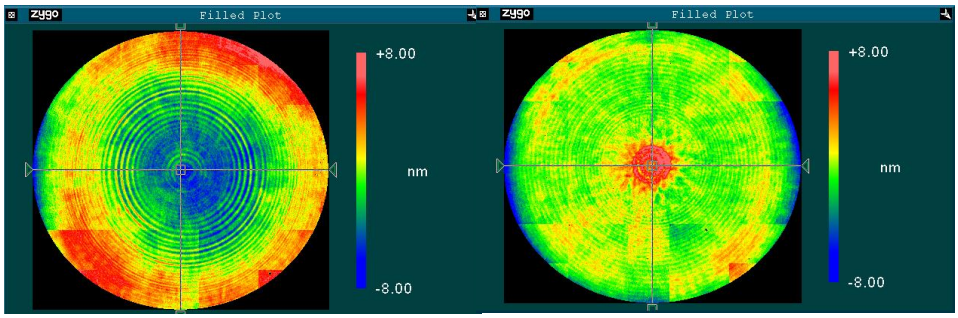

Figure 2. Typical flatness measured on an ELI-NP mirror after stress compensation.

These mirrors show an average flatness equal to 0.86 ± 0.17 λ/30 at 515 nm or an average sag of -14.73 ±2.97 nm over a 24×26 mm² aperture meaning that they are all within the requested specification. It is worth noting that while surface profile is not exactly identical to that of the substrate before coating, it is very close except next to the edge of the mirrors. This is probably due to non-uniformity of the coating and boundary effects. One can also see that the surface shows periodic rings. Such a structure is typical of the magneto-rheological polishing technique that was implemented in order to reach the specified flatness of the substrates. It is also interesting to note that the polishing tended to produce the same sign of sag (i.e. negative) for all the mirrors. As they will be used in-line, the residual sag will sum up when beam reflects on each mirror and will produce a curvature of the wavefront. To overcome this problem, we fabricated a batch of mirrors which should produce a -2 nm PtV curvature on the front face. Substrates were thus coated with an additional 90 nm silica layer before coating them with the mirror. Flatness was measured for each sample and an average sag of -16.73 ±3 nm over a 24×26 mm² aperture was measured (i.e. 2 nm smaller than that measured on perfectly compensated mirrors). This result shows that stress compensation could be, in average, controlled with a precision better than 1 nm. This result is a statistical result as each substrate before coating has a different flatness and shape.

A third batch of mirrors was fabricated. These mirrors have larger sizes up to 76.2 mm diameter. When reaching such a diameter, several parameters will influence the final flatness of the mirrors:

1. the original flatness of the substrate,
2. the accuracy of the stress compensation, which is influenced by the repeatability of two coating runs resulting in different layer thickness distribution and the possible variations of temperature during coating,
3. the uniformity of the coating.

Indeed, this last parameter will play a key role in the final flatness as the coatings thickness is pretty large (between 2.5 and 3 µm). Supposing that the first two parameters have no contribution to the final measured flatness, it can be easily shown that, in first approximation (i.e. without considering possible larger contribution associated with phase change at reflection [22,23]) maximum thickness change of the coating should not exceed 0.5%. In order to meet the last two criteria, the choice of PARMS technology is justified. Indeed, with such a technology, the uniformity over a 70 mm aperture is within ±0.2% and therefore compatible with the project specifications. An additional advantage of such a technology is the high repeatability of the deposition process that allows securing that the deposition

parameters are identical from one deposition to another, but also from the beginning to the end of the process.
Two types of mirrors were fabricated. A first batch with stress-compensation achieved by depositing the same mirror on the rear face (as for the 30 mm diameter mirrors), and a second one by depositing an antireflection coating. As the antireflection coatings have total thickness much smaller than the mirrors (Table 2), ~500 nm vs. 2.5-3 µm, stress compensation was obtained by adding a silica layer with adapted thickness, in between the substrate and the antireflection coating. That way, since the silica layer has a refractive index close to that of the substrate, the optical function is maintained. In addition, a precise stress compensation can be achieved and even adapted if the substrate has an original sag. Table 5 provides a summary of each type of mirrors.

Table 5. Average flatness performances of the large aperture mirrors.

Front side coating	Rear side coating	Diameter	Number of samples	Average flatness	Standard deviation flatness
Mirror	Mirror	50 and 75 mm	26	19.4 nm	4.3 nm
Mirror	Antireflection coating	50 and 75 mm	16	18.9 mm	5.3 mm

The average flatness of the mirrors is within the specified value (17 nm) and deviation is close enough to secure a flatness close to the specified one.

2.2 High performances bandpass filter

Another classical type of filters are bandpass filters. Two classes of filters were considered in this work. A first narrow bandpass filter (BPF1) dedicated to UV. Main specifications are:

- Central wavelength = 351 nm ± 2 nm
- FWHM = 20 nm ± 2 nm
- Average transmission > 90% over the spectral range [344 – 358] nm
- Blocking wavelength range: 200 nm – 1200 with OD ~ 3
- Flatness < 0.5 lambda @ 633nm
- Coating on back side: R < 1% on [340 - 360] nm
- Diameter = 50 mm
- Thickness = 5 mm

A second with broad bandpass (BPF2) in visible range, with main specifications:

- Cut-on wavelength (50% of peak transmission) = 380 nm ± 5 nm
- Cut-off wavelength (50% of peak transmission) = 745 nm ± 5 nm
- Average transmission > 90% over the spectral range 390 – 735 nm
- Blocking wavelength range: 200 nm – 355 nm and 770 nm – 1200 nm with OD ~ 3
- Flatness < 0.5 lambda @ 633nm
- Coating on back side: R < 1% on 375 – 750 nm
- Diameter = 50 mm
- Thickness = 5 mm

These filters were designed using a custom software that was developed internally in the lab. Main specifications of the designed filters are summarized in Table 5.

Table 5. Typical parameters of the designed bandpass filters.

Specifications	BPF1	BPF2
Substrate material	Fused silica	Fused silica
H material	HfO_2	Nb_2O_5
L material	SiO_2	SiO_2

Number of layers front face	170	34
Number of layer rear face	92	58
Thickness front side, µm	11.4	3.4
Thickness rear side, µm	13.7	3.5

Figure 3 illustrates the typical structures of each face (FF stands for front face and RF for rear face) of the BPF1. BPF1-FF is composed with 7 different periodic elementary structures, each associated with a different optical function. First two structures (S1 and S2) are quarterwave mirrors separated by matching layers in order to reject the wavelengths below 355 nm. Third structure (S3) is a three-cavity Fabry-Perot filters and last four structures (S4 to S7) are quarterwave mirrors separated by matching layers in order to reject the wavelength above 355 nm and up to 770 nm. BPF1-RF is composed with 3 different periodic structures (S8 to S10) each associated with a different optical function. Each structure is a quarterwave mirror, separated from the others by matching layers, and allows rejecting the wavelengths from 770 up to 1200 nm. In contrary to classical designs based on needle technique which result into complex designs [14,15], the implemented approach easily allows to split the coatings into elementary structures and thus to divide, in a custom way, the total coating between the two faces of the substrate.

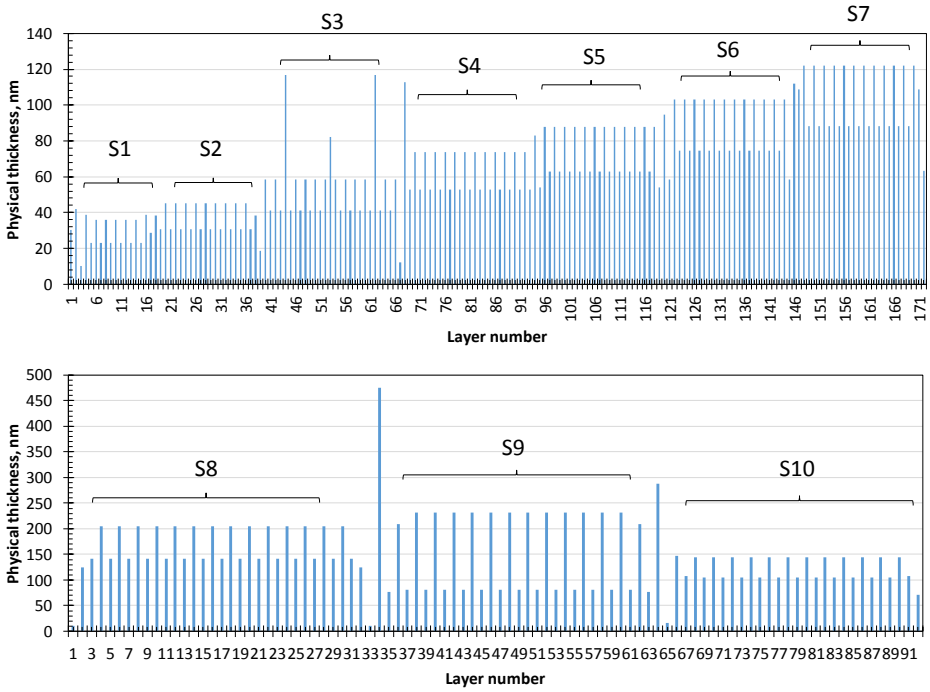

Figure 3. Typical structure of each face of the BPF1, top front face, FF and bottom rear face, RF. S1 to S10 represent each of the basic quarterwave structures composing the filter.

The high index material is different for each filter. BPF1 uses HfO_2 since the bandpass is situated in the UV region and requires high index material transparency in this region. In contrary, BPF2 uses Nb_2O_5 in order to decrease the total number of layers and rejection of the filter below 355 nm is achieved by the absorption of the Nb_2O_5 layers. Both faces of the substrates were coated with two different structrures. Front side secures the bandpass profile and part of the rejection while rear side secures high transmission in the bandpass region and broadband rejection. This is the same approach that has been previously implemented for this class of filters [9]. Indeed, based on the stress coefficient of each of the coating materials, we

made sure, during design, that stress induced deformation if very close for each of the coated surface. This approach secures a final flatness close to that of the uncoated substrates. For BPF1, stress induced deformation is equal to 2.5 µm (FF) and to 3.2 µm (BF) and for BPF2, stress induced deformation is equal to 614 nm (FF) and 664 nm (BF).

These filters were then fabricated. Table 6 presents the typical wavelengths used for monitoring each of the coatings.

Table 6. Typical wavelengths used for monitoring the two faces (front face, FF and rear face, RF) of the bandpass filters.

Coating	BPF1, FF	BPF1, RF	BPF2, FF	BPF2, RF
Number of monitoring glasses	6	3	1	4
Number of monitoring wavelengths	7	8	2	7

The BPF1-FF is composed with a sequence of 6 mirrors to allow complete rejection from 200 nm up to 770 nm in combination with a multi-cavity Fabry-Perot structure. Therefore, we used 6 different monitoring glasses associated with each of these individual structures. BPF1-RF is composed with 3 blocking mirrors that were monitored with a different glass. For each monitoring glass, different monitoring wavelengths could be used.

BPF2-FF produces the bandpass and the rejection up to 950 nm and BPF2-RF secures high transmission in the bandpass region and produces the rejection between 950 and 1200 nm. As there is no clear periodic structure, this filter being designed through a numerical approach, an optical monitoring strategy had to be determined. Due to a larger aperiodicity of the structure, the monitoring strategy developed for BPF2-RF was clearly more complex than that developed for BPF2-FF

The spectral performances of the fabricated filters were then characterized on the range from 200 up to 1200 nm (Figures 4 and 5).

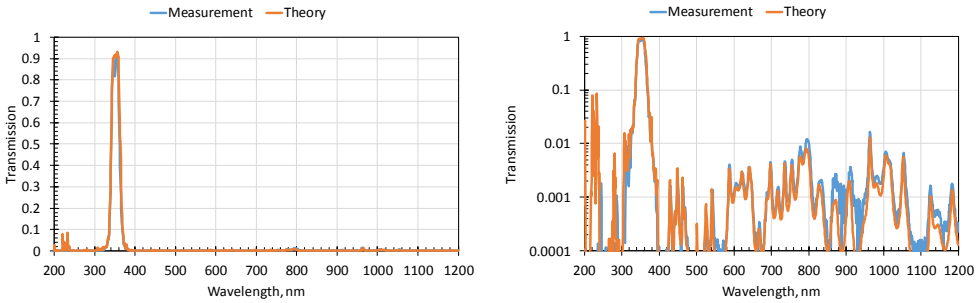

Figure 4. Spectral dependence of the transmission of BPF1 in linear and log scales. Theory is in orange and experimental data are in blue.

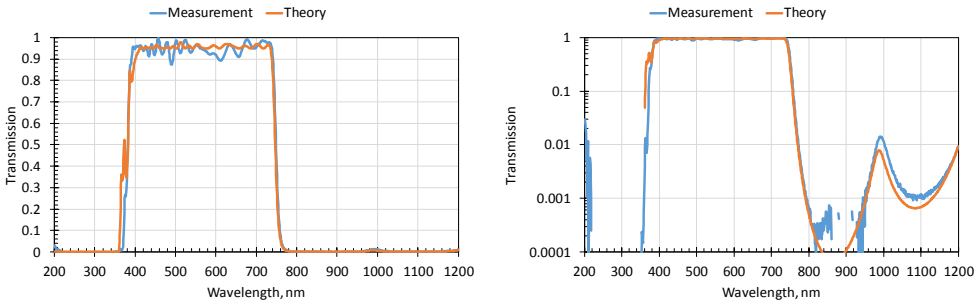

Figure 5. Spectral dependence of the transmission of BPF2 in linear and log scales. Theory is in orange and experimental data are in blue.

Close to theoretical performances could be achieved for both type of filters, confirming that the combination of a stable deposition process and an efficient optical monitoring strategy allows achieving high performance filters. Experimental rejection is almost overlapped with the theoretical one. In the bandpass, a ±5% deviation can be seen in both filters. This small difference reveals the higher sensitivity of the filter's performances in the high transmission regions than in the rejecting regions. But an analysis based on random errors show that the average error on the thickness of each individual layer does not exceed 1 %. Finally, a peak-to-valley flatness of λ @ 633 nm was measured on BPF1 and a flatness of λ/6 @ 633 nm was measured on BPF2 over a 45 mm aperture. In both cases, high flatness could be demonstrated. The better flatness of BPF2 can be easily explained by thinner stack designs and closer overall thickness of the structures of each face stacks. Indeed, we show in Figure 6 the typical flatness measured over a 25 mm aperture on a witness glass with BPF2-FF, BPF2-RF and BPF2-FF+RF. Very similar sag between1.3 and 1.4 µm could be measured on each single side coated test glass. Final flatness of the dual side coated optical filter is thus close to that of the original uncoated substrate.

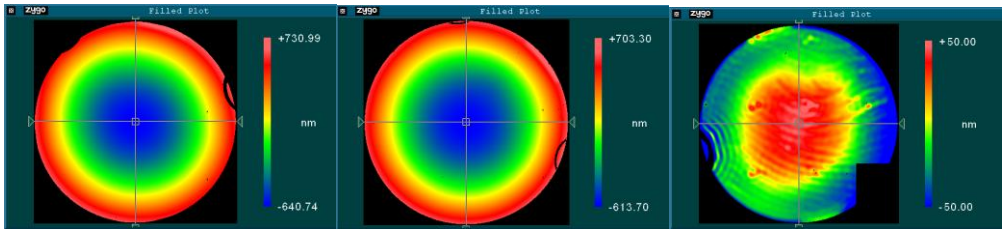

Figure 6. Measured flatness on a witness glass coated with BPF2-FF (left), a witness glass coated with BPF2-RF (center), and the final glass coated with BPF2-FF+RF (left).

2.3 Filters with broadband controlled transmission

The last class of filters that we demonstrated are filters with broadband controlled spectrum [16]. These filters are commonly combined with white light source in order to produce broadband illumination with constant spectral brightness. As a consequence, the transmission of these filters must reproduce the inverse of the intensity distribution of the broadband light source and eventually also take into account the spectral sensitivity of the detector that will be used for the measurement. Two similar filters were studied (EF1 and EF2). . Both filters must match a spectral profile designed in spectral range from 375 up to 750 nm and illustrated in Figure 7. These filters do not present a spectral profile that can be reproduced with classical stack formulae; therefore, they were numerically designed. The whole spectral function was designed on the front face of the substrate and a broadband antireflection coating was designed for the rear face. Table 7 provides the typical parameters of the designed Front Face structures as well as some information on the optical monitoring strategy that was determined for each filter.

Table 7. Typical parameters of the designed filters with broadband controlled transmission.

Specifications	EF1	EF2
Substrate material	Fused silica	Fused silica
H material	HfO_2	HfO_2
L material	SiO_2	SiO_2
Number of layers front face	30	67
Thickness front side, µm	2.3	4.9
Number of monitoring glasses	1	2
Number of monitoring wavelengths	2	4

In both cases, high index material was HfO_2 in order to reach a transmission close to 100% at 375 nm. Both filters require total thickness not exceeding 5 µm. EF2 requires a larger number of layers than EF1 due to lower required transmission over several hundreds of nanometers spectral bandwidth. Another consequence is a more complex strategy for EF2 than for EF1 due to the aperiodicity of the structure. This is compensated by the use of two different monitoring glasses that split the monitoring into two structures with complexity similar to that of EF1. Both filters were coated with an antireflection coating on the rear face of the substrate. The antireflection coating is the same for EF1 and EF2 and is composed with 4 layers for a total thickness of 260 nm. It is obvious that such an antireflection coating will not allow producing stress compensation. Therefore, similarly to the ELI mirrors that were fabricated with an antireflection coating on the rear face, we added a silica layer at the substrate – antireflection coating interface. The thickness of this layer was different for EF1 and EF2 and adapted to the designed structure of the front face to produce efficient stress compensation. Indeed, the sags on the front face were expected to be -334 nm for EF1 and -680 nm for EF2. After the depositions of EF1-FF and EF2-FF, the measured sags were -336 nm for EF1 and -598 nm for EF2. The silica layer thicknesses used for EF1 and EF2 were thus respectively equal to 1040 nm and 1840 nm.

These filters were then fabricated and spectral performances and flatness were measured (Figure 7).. Very good target / experimental agreement is again achieved for both filters. For EF1, maximum transmission à 375 nm is equal to 96.5%; an average deviation from theory of 1.3% and not exceeding 3.7% is obtained. For EF2, maximum transmission à 375 nm is equal to 96.5%; an average deviation from theory of 1.2% and not exceeding 10.3% (around 500 nm) is obtained. Finally, flatness of ~λ/6 @ 633 nm was measured on EF1 and EF2 over the 25 mm aperture.

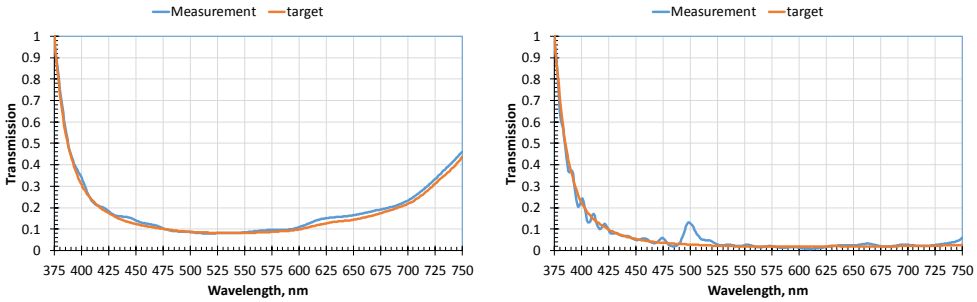

Figure 7. Spectral dependence of the transmission of EF1 (left) and EF2 (right). Theory is in orange and experimental data are in blue.

4. Conclusion

Various classes of high performance filters were demonstrated including mirrors, bandpass filters (narrowband and broadband) and filters with broadband controlled transmission. For

each type of filters, many design parameters were studied. Experimental demonstration was then carried out and close to theoretical performances were obtained. In addition, stress compensation using rear face coatings was demonstrated. This stress compensation is achieved with a simultaneous control of the spectral properties of the overall filters. High performances – high flatness filters were demonstrated showing that plasma-assisted reactive magnetron sputtering not only allows controlling the spectral properties of filters but also the final filters flatness to values close to that of original substrate flatness if properly designed.

Funding

This work was partially funded by ALSYOM company, CNRS-LAL and Bertin Technologies company.

References

1. Strauss G.N. (2003) Mechanical Stress in Optical Coatings. In: Kaiser N., Pulker H.K. (eds) Optical Interference Coatings. Springer Series in Optical Sciences, vol 88. Springer, Berlin, Heidelberg.
2. G. Stoney, The tension of metallic films deposited by electrolysis, Proc. R. Soc. London, Ser. A 82, 172 (1909).
3. G. Abadias, E. Chason, J. Keckes, M. Sebastiani, G. B. Thompson, E. Barthel, G. L.Doll, C. E. Murray, C. H. Stoessel, and L. Martinu, "Stress in thin films and coatings: Current status, challenges, andprospects," Journal of Vacuum Science & Technology A36, 020801 (2018).
4. Y. Wang, Y-G. Zhang, W.-L. Chen, W. Shen, X. Liu, and P.-F. Gu, "Optical properties and residual stress of YbF3 thin films deposited at different temperatures," Appl. Opt. 47, C319-C323 (2008)
5. M. Bischoff, T. Nowitzki, O. Voß, S. Wilbrandt, and O. Stenzel, "Postdeposition treatment of IBS coatings for UV applications with optimized thin-film stress properties," Appl. Opt. 53, A212-A220 (2014)
6. The VIRGO Collaboration, "The VIRGO large mirrors: a challenge for low loss coatings," Classical and Quantum Gravity 21(5), S935 (2004).
7. J. B. Oliver, P. Kupinski, A. L. Rigatti, A. W. Schmid, J. C. Lambropoulos, S. Papernov, A. Kozlov, C. Smith, and R. D. Hand, "Stress compensation in hafnia/silica optical coatings by inclusion of alumina layers", Opt. Express 20, 16596-16610 (2012)
8. M.-M. de Denus-Baillargeon, T. Schmitt, S. Larouche, and L. Martinu, "Design and fabrication of stress-compensated optical coatings: Fabry–Perot filters for astronomical applications," Appl. Opt. 53, 2616-2624 (2014).
9. T. Begou, H. Krol, D. Stojcevski, F. Lemarchand, M. Lequime, C. Grezes-Besset and J. Lumeau, "Complex optical interference filters with stress compensation for space applications", CEAS Space J 9(4), 441–449 (2017).
10. H. Liu, L. Jensen, P. Ma, D. Ristau, Stress compensated anti-reflection coating for high power laser deposited with IBS SiO2 and ALD Al2O3, Applied Surface Science 476, 521-527 (2019).
11. F. Lemarquis, "Athermal compensation of the stress-induced surface deflection of optical coatings using iso-admittance layers" Applied Optics, 53(4), 229-236 (2014).
12. T. Begou and J. Lumeau, "Accurate analysis of mechanical stress in dielectric multilayers", Optics Letters 42(16) (2017).
13. https://www.optilayer.com/
14. A. V. Tikhonravov, "Some theoretical aspects of thin-film optics and their applications," Appl. Opt. 32,4265–4275 (1993).
15. B. T. Sullivan and J. A. Dobrowolski, "Implementation of a numerical needle method for thin-film design," Appl. Opt. **35**, 5484-5492 (1996).
16. M. Vignaux, F. Lemarchand, T. Begou, C. Grèzes-Besset and J. Lumeau, "Automated method for the determination of the all-optical monitoring strategy of complex thin-film filters", Optics Express 27(9), 12373-12390 (2019).
17. L. Abel-Tiberini, F. Lemarquis, and M. Lequime, "Dedicated spectrophotometer for localized transmittance and reflectance measurements," Appl. Opt. **45**, 1386-1391 (2006)
18. www.eli-np.ro/
19. C. A. Ur, Gamma beam system at ELI-NP, AIP Conference Proceedings 1645, 237 (2015); doi: 10.1063/1.4909580
20. K. Cassou, C. F. Ndiaye, N. Beaugerard, K. Dupraz, F. Falcoz, D. Douillet, T. Le barillec, A. Martens, Y. Peinaud, H. Rocipon, A. Variola, and F. Zomer, "Laser Beam Circulator for the Generation of a High Brilliance Gamma Beam at ELI-NP," in High-Brightness Sources and Light-driven Interactions, OSA Technical Digest (online) (Optical Society of America, 2018), paper HW4A.7.
21. A. O'Keefe and D. A. G. Deacon, "Cavity ring- down optical spectrometer for absorption measurements using pulsed laser sources", Rev. Sci. Instrum.59, 2544 (1988).

22. P. Kupinski, H. A. Macleod, “Advances in optical manufacturing: measurement considerations when specifying optical coatings”, Laser Focus World, vol 51, 2015.
23. A. Piegari, A. Sytchkova, “Phase distortion and thickness variation in the design of optical coatings”, Proceedings SPIE Volume 10562, International Conference on Space Optics — ICSO 2016; 105621H (2017).